Contemporânea
Contemporary Journal
Vol. 4 N°. 7: p. 01-31, 2024
ISSN: 2447-0961

Artigo

PREPARATION, CHARACTERIZATION AND ANALYSIS OF NANOSCALE MORPHOLOGY OF POLY(VINYL ALCOHOL) FILMS ASSOCIATED WITH SILK FIBROIN FUNCTIONALIZED WITH COPAÍBA OLEORESIN

PREPARAÇÃO, CARACTERIZAÇÃO E ANÁLISE DA MORFOLOGIA EM NANOESCALA DE FILMES DE POLI(ÁLCOOL VINÍLICO) ASSOCIADOS COM FIBROÍNA DE SEDA FUNCIONALIZADA COM OLEORRESINA DE COPAÍBA

PREPARACIÓN, CARACTERIZACIÓN Y ANÁLISIS DE LA MORFOLOGÍA NANOMÉTRICA DE PELÍCULAS DE POLI(ALCOHOL VINÍLICO) ASOCIADAS CON FIBROÍNA DE SEDA FUNCIONALIZADA CON OLEORRESINA DE COPAÍBA

DOI: 10.56083/RCV4N7-203
Receipt of originals: 06/28/2024
Acceptance for publication: 07/19/2024

Daniel Sousa dos Santos
PhD student in Biodiversity and Biotechnology
Institution: Universidade Federal do Amapá (UNIFAP)
Address: Macapá, Amapá, Brasil
E-mail: danielsousa@unifap.br

Erveton Pinheiro Pinto
PhD in Biodiversity and Biotechnology
Institution: Universidade Federal do Amapá (UNIFAP)
Endereço: Macapá, Amapá, Brasil
E-mail: erveton@unifap.br

Nilson dos Santos Ferreira
PhD in Physics
Institution: Universidade Federal de Sergipe (UFS)
Address: São Cristóvão, Sergipe, Brasil
E-mail: nilson@academico.ufs.br

Irlon Maciel Ferreira
Phd In Organic Chemistry
Institution: Universidade de São Paulo (USP)
Address: Macapá, Amapá, Brasil
E-mail: irlon.ferreira@unifap.br

Arlefe Noite Ribeiro
Msc student in Environmental Sciences
Institution: Universidade Federal do Amapá (UNIFAP)
Address: Macapá, Amapá, Brasil
E-mail: arlefenoite@gmail.com

Adriana Maciel Ferreira
PhD in Biodiversity and Biotechnology
Institution: Universidade Federal do Amapá (UNIFAP)
Address: Macapá, Amapá, Brasil
E-mail: adriana.maciel@unifap.br

Ciro Augusto Fernandes de Oliveira Penido
PhD in Biomedical Engineering
Institution: Universidade Brasil (UNIVBRASIL)
Address: Macapá, Amapá, Brasil
E-mail: ciropenido@gmail.com

Robert Ronald Maguiña Zamora
PhD in Physics
Institution: Pontifícia Universidade Católica do Rio de Janeiro (PUC-RJ)
Address: Macapá, Amapá, Brasil
E-mail: robert@unifap.br

Tiago Marcolino de Souza
PhD in Materials Science and Engineering
Institution: Universidade Federal de São Carlos (UFSCAR)
Address: Macapá, Amapá, Brasil
E-mail: tiago.souza@ueap.edu

ABSTRACT: Biodegradable films based on poly(vinyl alcohol) (PVA) and bioactive substances have been receiving great attention in the food industry, as they offer an eco-friendly alternative to conventional packaging. In this context, we synthesized PVA (PVAF) films containing silk fibroin (SF) formulations functionalized with copaiba oleoresin (CO) for use as bioactive packaging. Four different formulations were prepared using the casting method, varying the SF-CO concentrations from 0 to 15% (v/v) in the PVA matrix. The samples were characterized regarding morphology, nanotexture, physicochemical, and barrier properties. SEM images revealed the uniform morphology of the films, and AFM data allowed the quantification of surface characteristics such as uniformity and homogeneity, confirming the uniform distribution of SF-OC in the PVA matrix. All films showed high water absorption power (more than twice their mass weight), and the incorporation of SF-CO did not change the water vapor permeability rate of PVAF. In contrast, the solubility of PVAF decreases with SF-CO content. FTIR and UV-

vis spectra confirmed the presence of SF-CO in PVAF and indicated possible intermolecular interactions between PVA and SF-CO. Finally, our findings suggest that the incorporation of SF-CO into the PVA matrix is a viable alternative for producing eco-friendly packaging.

KEYWORDS: PVA, copaiba oilresin, silk fibroin, polymeric films, bioactive packaging.

RESUMO: Filmes biodegradáveis à base de poli(álcool vinílico) (PVA) e substâncias bioativas têm recebido grande atenção na indústria alimentícia, pois oferecem uma alternativa ecológica às embalagens convencionais. Nesse contexto, sintetizamos filmes de PVA (PVAF) contendo fibroína de seda (SF) funcionalizada com oleorresina de copaíba (OC) para uso como embalagem bioativa. Quatro formulações diferentes foram preparadas utilizando o método de casting, variando as concentrações de SF-OC de 0 a 15% (v/v) na matriz de PVA. As amostras foram caracterizadas quanto à morfologia, nanotextura, propriedades físico-químicas e barreiras. Imagens de MEV revelaram a morfologia uniforme dos filmes e dados de AFM permitiram a quantificação das características de superfície, como uniformidade e homogeneidade, confirmando a distribuição uniforme de SF-OC na matriz de PVA. Todos os filmes mostraram alto poder de absorção de água (mais de 2 vezes o seu peso em massa) e a incorporação de SF-OC não alterou a taxa de permeabilidade ao vapor de água do PVAF. Em contraste, a solubilidade do PVAF diminui com o conteúdo de SF-OC. Espectros de FTIR e UV-vis confirmaram a presença de SF-OC no PVAF e indicaram possíveis interações intermoleculares entre PVA e SF-OC. Finalmente, nossos achados sugerem que a incorporação de SF-OC na matriz de PVA é uma alternativa viável para a produção de embalagens ecológicas.

PALAVRAS-CHAVE: PVA, oleorresina de copaíba, fibroína de seda, filmes poliméricos, embalagem bioativa.

RESUMEN: Películas biodegradables a base de poli(álcool vinílico) (PVA) y sustancias bioactivas han recibido gran atención en la industria alimentaria, ya que ofrecen una alternativa ecológica a los envases convencionales. En este contexto, sintetizamos películas de PVA (PVAF) que contienen fibroína de seda (FS) funcionalizada con oleorresina de copaiba (OC) para su uso como envase bioactivo. Se prepararon cuatro formulaciones diferentes utilizando el método de colada, variando las concentraciones de FS-OC de 0 a 15% (v/v) en la matriz de PVA. Las muestras fueron caracterizadas en cuanto a morfología, nanotextura, propiedades fisicoquímicas y de barrera. Imágenes de SEM revelaron la morfología uniforme de las películas, y los datos de AFM permitieron la cuantificación de las características de la superficie, como uniformidad y homogeneidad, confirmando la distribución

uniforme de SF-OC en la matriz de PVA. Todas las películas mostraron un alto poder de absorción de agua (más de 2 veces su peso en masa), y la incorporación de FS-OC no alteró la tasa de permeabilidad al vapor de agua del PVAF. En contraste, la solubilidad del PVAF disminuye con el contenido de SF-OC. Espectros de FTIR y UV-vis confirmaron la presencia de SF-OC en el PVAF y indicaron posibles interacciones intermoleculares entre PVA y FS-OC. Finalmente, nuestros hallazgos sugieren que la incorporación de SF-OC en la matriz de PVA es una alternativa viable para la producción de envases ecológicos.

PALABRAS CLAVE: PVA, oleorresina de copaíba, fibroína de seda, películas poliméricas, envase bioactivo.

1. Introduction

The use of eco-friendly materials for manufacturing packaging has become a necessity due to the enormous damage to the environment caused over the years. Poly (vinyl alcohol) (PVA) is one of the best-known polymers that has been presented as a viable alternative in the manufacture of packaging due to its excellent physical-chemical properties, such as viscosity, film formation, emulsification, dispersion power, tensile strength, flexibility, and gas barrier properties (Godovsky, 2000; Halima, 2016; Sathidevi, 2020). Furthermore, it is a biocompatible, thermostable, water-soluble, non-toxic, and biodegradable material in both aerobic and anaerobic conditions (Abdullah *et al*., 2017; Halima, 2016; Aslam *et al.,* 2018).

In this context, biocomposites are highly promising for various applications in the food industry and in the production of active packaging as they present innovative characteristics and biofunctional properties (Azeredo, 2009; Tao *et al*., 2017). The formation of active packaging is characterized by the incorporation of additives into the polymeric matrix with

the aim of maintaining or extending the quality and shelf life of the food product. Antioxidant, flavoring, antimicrobial, oxygen, and ethylene-absorbing substances are examples of active agents that, when present in the packaging, can interact with the food in order to delay the rate of deterioration of the product (Appendini; Hotchkiss, 2002; Mane, 2016; Wyrwa; Barska, 2017; Firouz *et al*., 2021).

The incorporation of antimicrobial agents in food packaging, for example, is one of the most promising alternatives for increasing the safety, stability, functionality, and shelf life of food products (Zhen *et al*., 2022; Var; Uzunlu, 2019; Ahmed *et al*., 2018).

In fact, the literature has been reporting the use of natural products as important bioactive agents that enhance the functional properties of PVA-based films for application as active and intelligent food packaging (Mustafa *et al*., 2021; Tanwar *et al*., 2021; Varghese *et al*., 2023; Kanatt *et al*., 2012). Given this, we can highlight the use of vegetable oils as a promising route for incorporating bioactivity into polymeric films (Pinto *et al.*, 2023; Rehman *et al*., 2020; Ju *et al*., 2019; Anis *et al*., 2021; Ghani *et al*., 2018; Bof *et al*., 2021).

Additionally, several biological properties have been attributed to copaiba oil, thus enabling pharmacological applications such as antimicrobial, antinociceptive, antineoplastic, anti-inflammatory, and healing, with potential for the treatment of skin diseases such as psoriasis, eczema, dermatitis, and leishmaniasis, among others (Veiga; Pinto, 2002; Yamaguchi; Garcia, 2014; Masson, 2011; Quemel *et a*l. 2021).

However, the incorporation of vegetable oils into film-forming solutions presents some challenges due to the following characteristics of these oils: hydrophobicity, volatility of some components, and sensitivity to environmental factors such as UV radiation, temperature, oxygen, pH, and humidity (Atarés; Chiralt, 2016). Therefore, to overcome these limitations,

vegetable oils are normally emulsified for subsequent dispersion in the film-forming solution.

Emulsification methods generally use copolymers and proteins as a viable alternative route to increase oil dispersion in aqueous vehicles (Echeverría; Albuquerque, 2019). In view of this, it is noteworthy that silk fibroin has been recommended in the literature as an alternative dispersing agent for various types of surfactants used in the formulation of emulsions, mainly due to its low production cost, low cellular and environmental toxicity, high biodegradability, and being a protein-based biomaterial (Ferreira *et al*., 2017).

Based on the above, the objective of this work was to prepare PVA (PVAF) films containing in their matrix a formulation of silk fibroin (SF) functionalized with copaiba oleoresin (CO) for a possible application as active packaging. Thus, the influence of SF-CO content on the morphological properties, nanotexture, physicochemical, and barrier properties of PVAF was investigated.

2. Methodology

2.1 Materials

Silkworm cocoons, species Bombix mori L., and poly(vinyl alcohol) (PVA) with a degree of hydrolysis of 89–98 were purchased from Sigma Aldrich (Brazil). Copaíba oleoresin (CO) was purchased from local commerce (Macapá, Amapá, Brazil). Isopropyl alcohol and ethanol were purchased from Synth (Brazil). All the products mentioned were used without further purification. The aqueous solutions used in the experiments were produced with distilled or deionized water, and all other chemicals were of analytical grade.

2.2 Fibroin Extraction

The silk fibroin solution was prepared based on the method developed by Ferreira *et al*. (2017). Initially, 3 g of silkworm cocoon was chopped and transferred to a solution of 500 mL of 2% Na_2CO_3. Then, the solution was heated to a temperature of 100 °C and maintained under magnetic stirring for 30 min, until fibrous material resulted. After this step, the fibers were washed with distilled water (3 x 1000 mL) and dried in an oven at 70 °C for 24 h. Subsequently, the fibroin fibers were solubilized by adding 50 mL of a three-part solution of H_2O:EtOH:$CaCl_2$ (proportion 8:2:1 M). This solution was maintained at 80 °C for 6 hours with magnetic stirring. Finally, the solution was then dialyzed for 3 days at room temperature, with the dialysis water being changed every 24 hours. To remove larger particles or impurities, the fibroin solution was centrifuged at 75 xg for 10 min and stored at 10 °C at a concentration of 2% (v/v).

2.3 Preparation of the Bioactivated Fibroin Formulation with Copaiba Oleoresin (CO)

A formulation was prepared according to the methodology proposed by Tavares-Dias *et al*. (2021), with a final volume of 10 mL and containing the following constituents: 25% silk fibroin solution, 5% CO, 25% isopropanol, and 45% distilled water. Initially, an organic phase was prepared by adding the compounds CO and isopropanol in a glass bottle (15 mL). Then, the mixture was stirred using a magnetic stirrer (35 x g) for 3 minutes. The aqueous phase (silk fibroin and H2O) was then added, with a flow rate of approximately 0.5 mL/min and continuous stirring for 60 min. The resulting product was stored at 18 °C and named the fibroin-copaiba oil (SF-CO) formulation.

2.4 Film Production

Poly(vinyl alcohol) (PVA) was solubilized in 200 mL of deionized water with the aid of a mechanical stirrer at 300 rpm in a water bath at 90 °C for 1 hour at a concentration of 5% (m/v). When the aqueous medium showed homogeneous gelatinization, the film-forming solution was removed from the water bath and stirred until it reached 40 °C. Then, the SF-CO formulations were added to the medium at concentrations of 5%, 10%, and 15% in relation to the mass of PVA (Board 1) under magnetic stirring for 30 min until the solution was completely homogeneous. Subsequently, 20 g of the mixture was poured onto petri dishes (9.5 cm in diameter) in a standardized way for drying and subsequent film formation (Guimarães JR *et al*. 2018). Drying took place over 24 hours in a digital air circulation oven at 40 °C (SOLAB Ar).

Board 1. Formulations of the synthesized films.

Formulation	PVA (% m/v de H_2O)	SF/CO (% m/m de PVA)
PVA	5	0
PVA1	5	5
PVA2	5	10
PVA3	5	15

Source: Prepared by the authors, 2024.

2.5 Characterization of the Films

2.5.1 Thickness

The thickness of the films was measured using a digital micrometer MDC-25SX (Mitutoyo, Japan) with a resolution of 0.001 mm and defined by the average of five random measurements in different parts of the same sample.

2.5.2 Hygroscopicity and water solubility

Hygroscopicity and water solubility were calculated according to the methodology proposed by Sun *et al*. (2022) with adaptations, where pieces of the films obtained were cut (20 × 20 mm in area) and weighed to obtain the dry mass of the film (W1). Next, the weighed samples were submerged in 20 mL of deionized water, remaining in this condition for 24 hours at room temperature. Subsequently, the samples were removed from the water, and absorbent paper was used to remove surface water. The wet films were weighed, and the wet mass was called W2. Then, the samples were dried at 45 °C for another 24 hours and weighed, with their final mass recorded as W3. Each sample was evaluated in triplicate, and the average value was calculated. The water absorption rate (A) was calculated using Equation 1.

$$\%A = \left[\frac{W_2 - W_3}{W_3}\right] \times 100 \quad (1)$$

Similarly, water solubility (S) was calculated using Equation 2.

$$\%S = \left[\frac{W_1 - W_3}{W_1}\right] \times 100 \quad (2)$$

2.5.3 Water vapor permeability rate

The water vapor permeability (WVP) property was calculated gravimetrically at 25 °C, according to the ASTM E96/E96M-13 standard with minor modifications and with the methodology proposed by Scatolino *et al*. (2022). The films were fixed to the opening of amber glass bottles (18 mm diameter opening) for vapor permeability, containing 10 mL of distilled water. These sets were weighed, placed inside a desiccator containing blue silica gel, and stored at 25 °C and 50% RH in an incubator. The masses were

weighed at 24-hour intervals over 9 days. Variations in the mass of each permeation set were plotted as a function of time and evaluated using linear regression. From the straight line obtained, the angular coefficient (g/t) was determined, and the water vapor transmission rate (WVTR) was calculated, according to Equation (3).

$$WVTR = (g/t)/A \quad (3)$$

where A is the sample permeation area (m²).

2.5.4 Fourier transform infrared (FTIR) spectroscopy

To obtain FTIR spectra, an FTIR spectrometer (excitation wavelength 1064 nm) with a diamond plate attenuated total reflection sampling accessory (Spectrum Two FT PerkinElmer, Inc., Waltham, MA, USA) and a deuterated triglycine sulfate detector were used. The spectral range was set between 450 and 4000 cm^{-1} and the resolution was set at 0.5 cm^{-1}.

2.5.5 UV–Vis spectroscopy

The ultraviolet-visible (UV-Vis) spectra of the films were recorded using a UV-Vis spectrophotometer (VARIAN, Cary 100). The range for scans was in the spectral range of 200–800 nm. The test was repeated three times for each sample.

2.5.6 Scanning electron microscopy

The morphology of the films was evaluated using a scanning electron microscope (SEM) (TM3030Plus Tabletop Microscope, Hitachi, Japan). The

scans were carried out under ambient conditions using a voltage of 5 kV to avoid damaging the sample.

2.5.7 Atomic force microscopy

The topography of the films was evaluated using an atomic force microscope (AFM) (model EasyScan 2, Nanosurf, Switzerland) in tapping mode and under environmental conditions (25 °C and 51% RH). The scans were performed with a silicon probe (Tap190AL-G, Nanosurf, Switzerland) and a cantilever made of the same material, with an elastic constant and resonance frequency of 48 N. m^{-1} and 190 kHz, respectively. The tapping mode was programmed with an amplitude of 30.39 nm, a setpoint of 21.05 nm, and a scan rate of 1 Hz. The resolution was 256 pixels per line in an image formed by 256 lines. The films were cut into 1 cm^2 sizes and fixed to the sample holder with double-sided adhesive tape. Three randomly chosen areas (40 μm^2) of each film were scanned.

2.5.8 Moran global index and topographic entropy

The analysis of the spatial autocorrelation of heights on the surface of the films was carried out by calculating the Moran global index (I) (Equation 4), according to the methodology proposed by Pinto *et al*. (2021).

$$I = \frac{N}{\sum_i \sum_j W_{ij}} \frac{\sum_i \sum_j W_{ij}.(z_i-\mu).(z_j-\mu)}{\sum_i (z_i-\mu)^2} \quad (4)$$

where N is the total number of areas analyzed, W_{ij} is the connectivity matrix (queen type) between the areas, Z_i and Z_j are the heights in areas i and j, and μ is the average height of the real image. Moran correlograms were

generated using the *sp.correlogram* function from the spdep package written in the R programming language.

To evaluate the global surface uniformity, we compute the topographic entropy (E_T) using Equations 5 and 6, as previously described in the literature (Pinto et al., 2023b).

$$E_T = \frac{\Lambda^{(2)} - {\Lambda_{min}}^{(2)}}{{\Lambda_{max}}^{(2)} - {\Lambda_{min}}^{(2)}} \quad (5)$$

$$\Lambda^{(2)} = -\sum_{i=1}^{N}\sum_{j=1}^{N} p_{ij} \cdot \log(p_{ij}) \quad (6)$$

where $\Lambda^{(2)}$ is the Shannon-based entropy, p_{ij} is the probability of each matrix element not being an outlier of the height distribution and N is the total number of pixels.

2.5.9 Fractal dimension

The fractal dimension of the AFM image was estimated using the box-counting algorithm through the Gwyddion software (http://gwyddion.net/download.php), according to Equation 7.

$$N(s) = \alpha \cdot s^{-D_F} \quad (7)$$

where N(s) is the minimum number of squares of side s needed to completely cover the set of black pixels in the binarized image, D_F is the fractal dimension, and α is a proportionality constant.

2.5.10 Lacunarity spectrum

The lacunarity exponent (β) of the AFM image was estimated by combining the glinding-box algorithm with the OTSU algorithm through a script implemented in R language by Pinto *et al*. (2021), according to Equations 8, 9, and 10.

$$\eta = \frac{{\sigma_B}^2}{{\sigma_T}^2} \tag{8}$$

$$L(p,r) = \frac{\sum p^2 \cdot Q(p,r)}{[\sum p \cdot Q(p,r)]^2} \tag{9}$$

$$L(p,r) = \alpha \cdot r^{-\beta} \tag{10}$$

where η, σ_B^2, and σ_T^2 are the Otsu separability, the variance between classes (separated by the selected threshold), and the variance of the heights in real image, respectively; L(p,r) is the fractal lacunarity; p is the number of lacunar pixels identified by Otsu binarization using the threshold that maximizes η; Q(p,r) is the probability distribution of lacunar pixels inside a box of side length r; and α is a proportionality constant.

2.5.11 Fractal succolarity

Fractal succolarity (S_F) was estimated using the box-counting algorithm, choosing a box of size 1 pixel, similar to the methodology proposed by Melo and Conci (2011) and later implemented in the R language by Pinto *et al.* (2018), according to Equation 11.

$$S_F = \frac{\sum_{k=1}^{n} P_r(k).P_0(k)}{P_0(n).\sum_{k=1}^{n} Pr(k)} \tag{11}$$

where $P_0(n)$ corresponds to the total number of boxes per line, while $P_r(k)$ represents the abscissa of the pressure centroid, referring to each box that can be occupied in the binarized image, and $P_0(k)$ is the number of boxes occupied per line. The SF was calculated in the top-down direction.

2.5.12 Statistical analysis

The results obtained were expressed as means and standard deviations, organized, according to relevance, in tables, graphs, charts, and figures. Significant differences between results were evaluated using one-way ANOVA and Tukey's test ($p < 0.05$) in Jamovi software version 1.8 (https://softradar.com/jamovi/).

3. Results and Discussions

3.1 Physical Characterization of the Films

Macroscopically, all films presented a transparent and continuous appearance, no rips, and easy handling, indicating a uniform dispersion of the SF-CO formulation in the PVA matrix.

The thicknesses of the films containing SF-CO (PVA1, PVA2 and PVA3) were significantly greater in relation to the formulation containing only PVA (Table 1). In general, films synthesized by the casting method have heterogeneous thicknesses as a characteristic (Pinto, *et al.* 2018).

Table 1. Thickness, hygroscopicity (A), solubility (S) and water vapor permeability rate (WVTR) of the films.

	Samples			
Propriety	**PVA**	**PVA1**	**PVA2**	**PVA3**
Thickness (μm)	93.6 ± 16.0^a	203.6 ± 2.4^b	193.2 ± 2.1^c	185.0 ± 3.0^d
A (%)	244.1680 ± 1.6108^a	239.3313 ± 1.2106^b	224.2307 ± 1.0174^c	213.8643 ± 0.9238^d

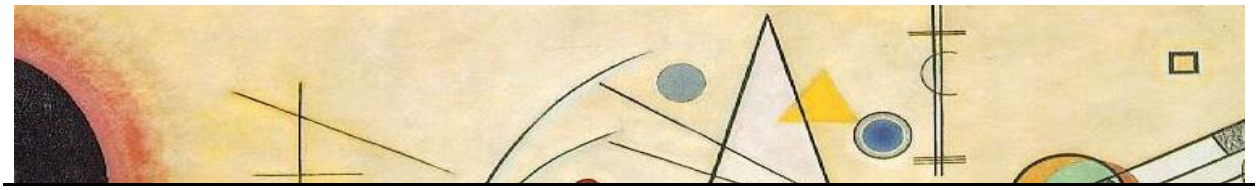

S (%)	16.3053 ± 0.1526[a]	13.1713 ± 0.1107[b]	12.2177 ± 0.0961[c]	11.7908 ± 0.0887[d]
WVTR (g/h.m²)	0,1158 ± 0,0045[a]	0,1111 ± 0,0050[a]	0,1100 ± 0,0048[a]	0,1189 ± 0,0054[a]

Source: Prepared by the authors, 2024. Different letters on the same line indicate a significant difference between the means by ANOVA and Tukey's test ($p < 0.05$).

Hygroscopicity is related to the ability of materials to absorb water, while solubility is related to their ability to dissolve in water. It was observed that both hygroscopicity and solubility decreased as the concentration of SF-CO increased (Table 1).

The decrease in these properties may be related to the presence of SF-CO in the films, which may add a more hydrophobic character due to the characteristics of the oil. Another factor that may have influenced the decrease in hygroscopicity and solubility of the films is the reduction of free OH groups due to the formation of hydrogen interactions between the layers of the PVA polymer matrix and the silk fibroin structure (Kuchaiyaphum *et al*., 2014).

The average water vapor permeability rates (WVTR), according to ANOVA and Tukey's test ($p<00.5$), did not show statistically significant differences between the samples.

3.2 Fourier Transform Infrared (FTIR) and UV-vis Spectroscopies

FTIR analysis (Figure 1) was used to identify the presence of functional groups OH-, C-O, and C-H in the chemical structure of the films, as these peaks indicate the existence of compounds such as phenolic acids, terpenoids, or flavonoids (Barbalata-Mândru *et al*., 2022). The FTIR spectra of the samples are very similar; however, the intensities and widths of the peaks showed differences, suggesting possible intermolecular interactions between the PVA polymeric matrix and the SF-CO formulation. The band between 3500 and 3200 cm^{-1}, with maximum intensity recorded at 3277

cm^{-1}, was attributed to v(O-H) stretching vibrations and the vibration of intermolecular hydrogen bonds, existing in the hydroxyl bonds of silk fibroin and PVA (Tao *et al*., 2017).

Figure 1. FTIR spectrum of PVA, PVA1, PVA2, and PVA3 films.

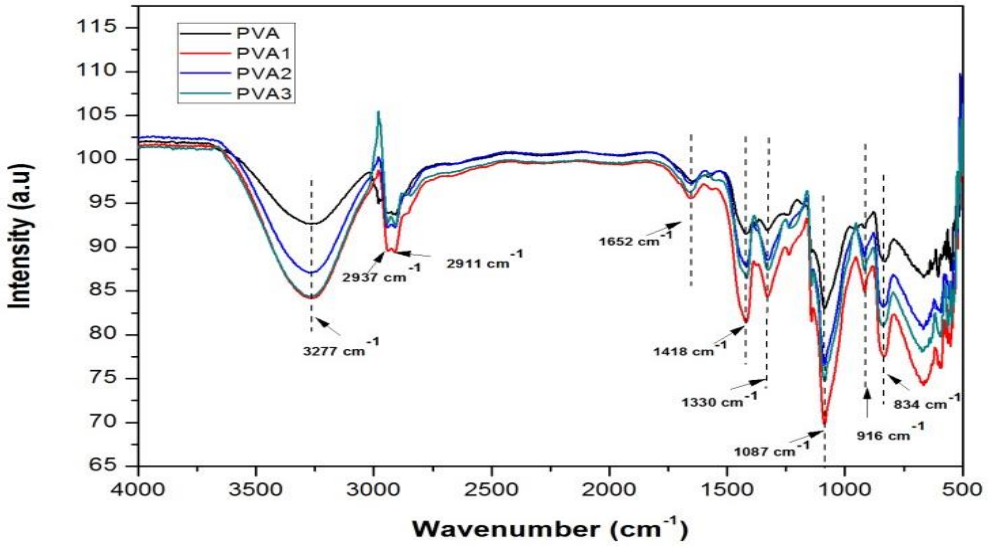

Source: Prepared by the authors, 2024.

The peaks at 2937 cm^{-1} and 2911 cm^{-1} correspond to asymmetric and symmetric v(C-H) stretching vibrations of -CH_1 and -CH_2 groups, respectively (Pavia *et al*., 2010). In films PVA1, PVA2, and PVA3, the changes in the stretching frequencies v(C-H) are evident, from 2937 cm^{-1} to 2911 cm^{-1}, causing an elongation of the peaks. Recent research indicates that the increase in intensity and change in the shape of the characteristic peaks for this vibration mode may be related to the presence of terpenoids incorporated into the polymeric matrix (Das et al., 2021).

Additionally, similar peaks were observed in all films at 1652 cm^{-1}, corresponding to stretching vibrations v(C=C), as well as at 1418 cm^{-1} and 1330 cm^{-1} attributed to bending vibrations δ(O-H) and δ(C-H), respectively. The peak in the region of 1087 cm^{-1} is due to stretching vibrations v(C-O) which may be related to the presence of secondary alcohols. The peak at 916 cm-1 corresponds to the stretching vibration of the v(C-O and C-C) groups,

while the characteristic peak at 834 cm^{-1} refers to C-C bonds (Lima, *et al*. 2016; Olewnik-Kruszkowska *et al*., 2019) . Some of the bands present in the FTIR spectrum of the pure PVA film show greater intensity in the PVA1, PVA2 and PVA3 films. This may be related to the presence of copaiba oil in the films, as its bands present characteristic frequencies for the functional groups at 2922 cm^{-1}, ν(-CH); 2854 cm^{-1}, ν(-CH2); 1743 cm^{-1}, ν(-C=O); 1415 cm^{-1}, δ(-CH), corroborating the hypothesis that there were intermolecular interactions in the composite film synthesis process (Pinheiro *et al*., 2017).

The results from the analysis of the UV-vis spectra are presented in Figure 2. The research data covers peaks in the range of 250–350 nm, which are characteristic of phenolic compounds and functional groups such as carbonyls that are present in those containing copaiba oil, confirming the effectiveness of impregnating the films with the oil. The literature reports that these natural compounds typically present certain absorption peaks in the ultraviolet light range (Parlinska-Wojtan *et al*., 2016; Wyrostek *et al*., 2020; Masłowski *et al*., 2021).

Figure 2. UV-VIS spectra characterization of the films.

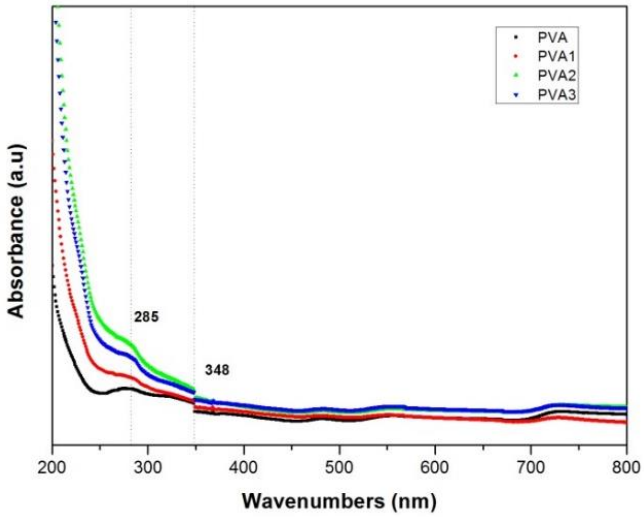

Source: Prepared by the authors, 2024.

Thus, the information recorded from the UV-VIS spectra of the PVA, PVA1, PVA2, and PVA3 films refers to the absorbance peaks observed at 285 and 348 nm and suggests the presence of phenolic compounds such as terpenoids, flavonoids, phenolic acids, or tannins present in the polymeric matrices of the PVA1, PVA2, and PVA3 film samples (Pavia *et al*., 2010).

Furthermore, it can be noted that the light absorption intensity gradually decreases for longer wavelengths, indicating that the samples are transparent in the visible region. Based on these results, it can be inferred that the films exhibit good optical transparency in the visible region, which is a desirable property for food packaging applications as it indicates good UV light stability of the material and can potentially extend the shelf life of the packaged product.

3.3 Scanning Electron Microscopy

The images obtained by SEM are presented in Figure 3 and show that all the films obtained presented a uniform texture with a continuous and smooth surface and did not present the presence of large pores or fissures, in addition to demonstrating few apparent flaws, in accordance with what was observed by Carvalho *et al*. (2019).

Figure 3. SEM images of the films: (a) PVA, (b) PVA1, (c) PVA2, and (d) PVA3.

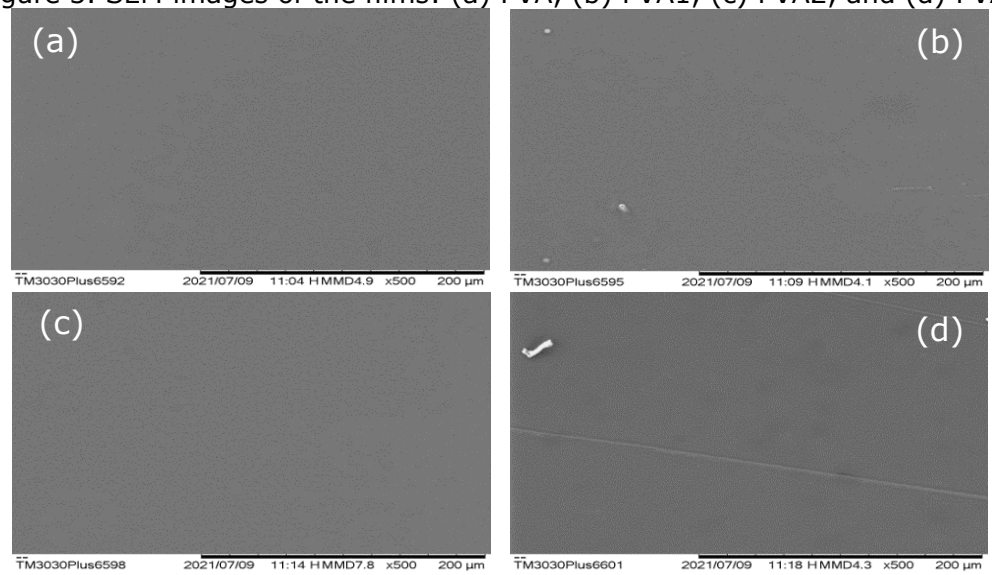

Source: Prepared by the authors, 2024.

Compared to the other samples, the PVA, PVA1, and PVA2 films exhibited the fewest surface irregularities, showing the most homogeneous surface. The PVA3 film presented more surface alterations due to interactions between the SF/OC and the poly(vinyl alcohol) polymer matrix, causing more pronounced micro-deformations and roughness on its surface.

Similarly, Li *et al*. (2019) reported that the encapsulation of turmeric essential oil in chitosan films caused heterogeneity and roughness in the films. Finally, it can be observed that the films presented a homogeneous structure in their polymeric matrix, which, according to the literature, represents a good indicator of the film's structural integrity and contributes to achieving good mechanical properties (Galdeano *et al*., 2013).

3.4 Nanoscale Morphology Analysis

Figure 4 presents the AFM images obtained from the films. The image data enabled the study of nanoscale topography, allowing for the evaluation of the height distribution of the pixels that spatially compose the microscopic texture of the surface (Figure 4).

Figure. 5. AFM topography of the composite films: (a) PVA, (b) PVA1, (c) PVA2, and (d) PVA3.

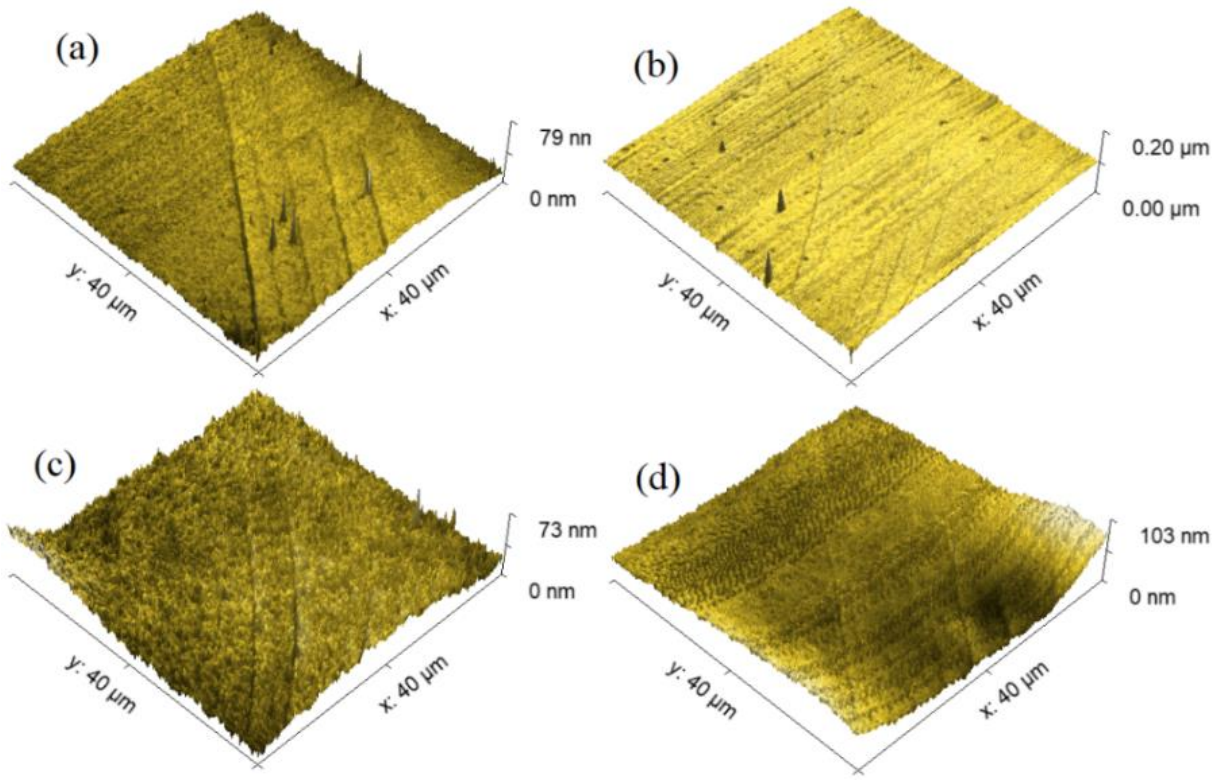

Source: Prepared by the authors, 2024.

From the analysis of the AFM images, it was evident that the concentration of SF-OC influenced the topographic characteristics of the surface of the films. In fact, it is possible to see that as the concentration of SF-OC in the polymer matrix of the film increases, its topography undergoes transformations in the physical surface parameters (Table 4). Furthermore, the height histogram (Figure 5) shows that the films have different height distributions.

Figure 5. Histogram of the topography of the composite films: (a) PVA, (b) PVA1, (c) PVA2, and (d) PVA3.

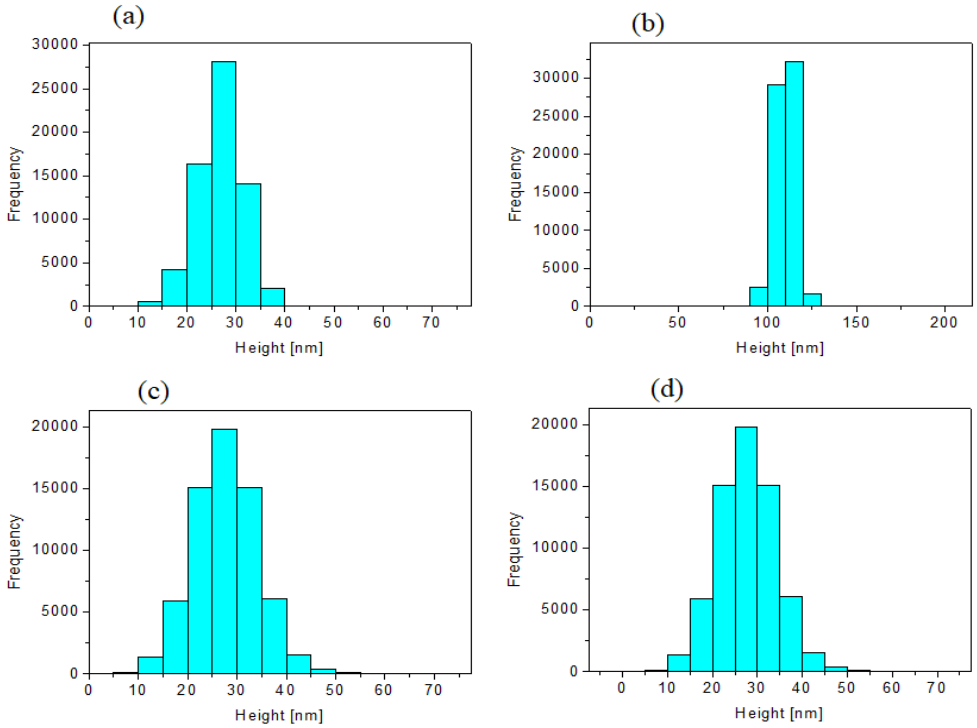

Source: Prepared by the authors, 2024.

Table 4. Surface parameters of the films composition.

Paramters	Symbol	(unidade)	PVA	PVA1	PVA2	PVA3
Root mean square height	Rrms	(nm)	4.676 ± 0.097[a]	5.289 ± 0.154[a]	6.416 ± 0.285[b]	12.096 ± 0.263[c]
Moran index for first neighborhood	I_{Lag1}	(-)	0.702 ± 0.055[a,c]	0.325 ± 0.014[b]	0.671 ± 0.035[c]	0.854 ± 0.014[a]

Source: Prepared by the authors. Different letters on the same line indicate a significant difference between the means by ANOVA and Tukey's test ($p < 0.05$).

The roughness Rrms, which numerically is the standard deviation of the heights on the surface of the PVA film, increases proportionally with the concentration of SF-OC. In fact, the PVA3 film was the roughest (Rrms~12.1 nm), while the control film (PVA) presented the lowest roughness value (Rrms~4.7 nm).

The uniformity of the set of height values recorded by the AFM can be evaluated through the topographic entropy (ET), which in practice is the

normalized Shannon entropy (TĂLU *et al*., 2020) of the data. The values of Et vary from zero to one, with Et = 1 representing a perfectly uniform set. Thus, the results showed that the PVA3 film has the least uniform surface area (Et~0.93); however, all films presented ET > 0.9.

The ILag1 of the correlograms in Figure 6, which represents a quantitative measure of short-range correlation, suggests that the PVA (ILag1 = 0.702), PVA2 (Ilag1 = 0.671), and PVA3 (ILag1 = 0.854) films have similar, more clustered heights. That is, they have a positive correlation in the spatial distribution of heights on the surface. This type of behavior is characteristic of self-affine fractal structures (Pinto *et al*., 2023).

3.5 Fractal analysis

The Moran correlograms (Figure 6a) confirmed the fractal behavior of the surface of the films on some length scales, which allows the evaluation of self-affinity patterns in the spatial distribution of heights recorded by AFM. A self-affine surface is one that presents statistical characteristics that are maintained in different parts and length scales throughout the surface structure (Mandelbrot, 1983; Pinto *et al*., 2021).

Figure 6. Autocorrelation Analysis and Lacunarity Analysis: (a) Moran's Correlogram and (b) Lacunarity exponent.

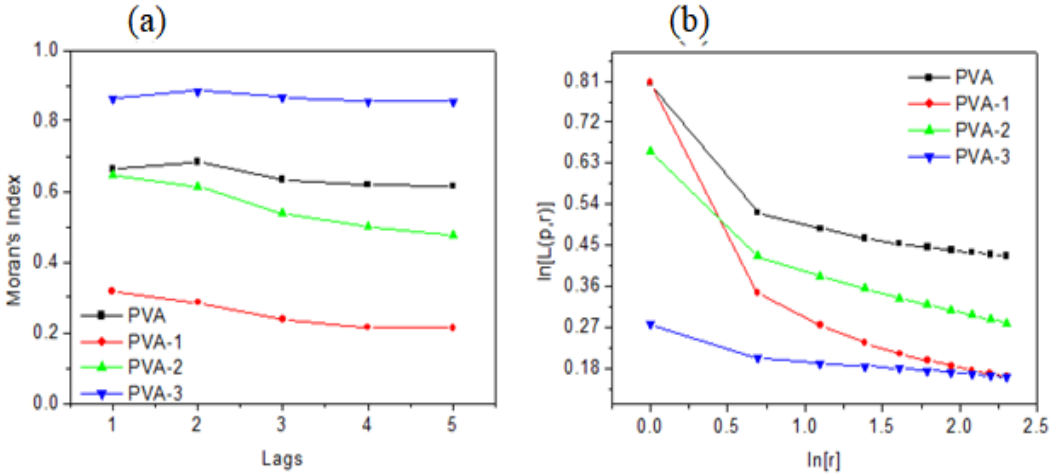

Source: Prepared by the authors, 2024.

In this context, the fractal dimension (D_F) values in Table 5 show that the films have similar complexity in height distribution, since the analysis of variance indicated a statistical difference in relation to the control only for the PVA2 film (D_F ~ 2, 4). Df measures the degree of complexity of the height distribution on the surface, and the higher the value, the more filled the texture metric space is, as well as the fact that the surface has a domain of higher spatial frequencies. Furthermore, a large value of D_F indicates that surface features are more persistent at different length scales.

Table 5. Fractal Parameters of the Films

Parameters	PVA	PVA1	PVA2	PVA3
D_F	2.368 ± 0.027^{a,b}	2.313 ± 0.011^{a}	2.428 ± 0.018^{b}	2.38 ± 0.011^{a,b}
S_F	0.431 ± 0.023^{a}	0.466 ± 0.023^{a}	0.516 ± 0.021^{a}	0.764 ± 0.030^{b}
β	0.127 ± 0.014^{a}	0.222 ± 0.020^{b}	0.156 ± 0.017^{a,c}	0.046 ± 0.004^{d}

Source: Prepared by the authors, 2024. Different letters on the same line indicate a significant difference between the means by ANOVA and Tukey's test ($p < 0.05$).

Fractal succolarity (S_F), on the other hand, is correlated with the phenomenon of percolation (Tălu *et al.,* 2020; De melo; Conci, 2008). For the measurements performed here, the connection between the upper and

lower bands of the AFM image was evaluated. Thus, the higher the S_F value, the greater the connection between the image bands. In view of this, the results suggest that only the PVA3 film (S_F ~0.8) presents greater percolation than the PVA control film (S_F ~0.4).

Another important fractal parameter to be considered is the lacunarity exponent β, the angular coefficient of the linear fit of the curves in Figure 6b. According to Pinto *et al*. (2021), lacunarity is a measure that assesses the heterogeneity of the distribution of vacancies on the film's surface, with β = 0 indicating that the lacunar distribution is exactly the same across the entire surface. Therefore, the surface of the PVA3 film is the most homogeneous (β~0.046), while that of the PVA1 film has greater heterogeneity (β ~ 0.222).

In this context, regarding the feasibility of producing active packaging, fractal analysis can be useful for evaluating the roughness and homogeneity of the film surfaces. For example, a film with a more homogeneous and less rough surface may be more suitable for application in active packaging. Additionally, a low lacunarity exponent can be an interesting indicator to ensure a uniform distribution of components on the film surface, which is important to guarantee the effectiveness of the active compound in the packaging.

4. Conclusion

PVA films functionalized with silk fibroin formulations combined with copaiba oil-resin were successfully produced. The resulting films exhibited a transparent appearance and a uniform surface. FTIR and UV-VIS analyses indicated that the SF-OC formulation chemically interacted with the PVA matrix and suggested the presence of natural compounds characteristic of copaiba oil-resin within the film matrices.

SEM analyses indicated a uniform morphology without significant flaws or cracks in the films obtained, which can be a good indicator of the structural integrity of the material. AFM analysis demonstrated that the films possess self-affinity characteristics as well as uniformity and homogeneity, corroborating the SEM images. Thus, based on the results obtained, it is possible to conclude that the incorporation of SF-OC into PVA films significantly affects the surface, correlation, and fractal properties of the films. In particular, the average roughness value (Rrms) increases with the increase in SF-OC concentration. Additionally, D_F presents higher values for the PVA1 and PVA3 formulations, indicating a greater fractal complexity of the surface of these films.

The autocorrelation and uniformity analysis showed that the incorporation of SF-OC also affects the correlation between different regions of the film surface, with lower values of I and ET observed for the PVA3 formulation compared to the other formulations. These results indicate that the addition of SF-OC can produce PVA films with interesting surface and fractal properties, which may be useful in the production of active packaging.

Finally, based on the data presented, the PVA2 sample would be the most suitable for use in packaging, considering the fractal characteristics as additional indicators. This is because the PVA2 sample shows higher D_F values, reflecting a more uniform surface, indicating greater spatial filling and persistence of surface characteristics across various scales.

Acknowledgements

We would like to thank the CNPQ agency for the financial support of the Academic Doctoral Scholarship for Innovation (DAI) number 140678/2023-9.

References

ABDULLAH, Z. W. *et al*. PVA, PVA blends, and their nanocomposites for biodegradable packaging application. **Polymer-Plastics Technology and Engineering**, v. 56, n. 12, p. 1307-1344, 2017.

AHMED, J. *et al.* Active chicken meat packaging based on polylactide films and bimetallic Ag–Cu nanoparticles and essential oil. **Journal of Food Science**, v. 83, n. 5, p. 1299-1310, 2018.

ANIS, A.; PAL, K.; AL-ZAHRANI, S. M. Essential oil-containing polysaccharide-based edible films and coatings for food security applications. **Polymers**, v. 13, p. 575, 2021. Disponível em: https://doi.org/10.3390/polym13040575.

APPENDINI, P.; HOTCHKISS, J. H. Review of antimicrobial food packaging. **Innov. Food Sci. Emerg**., v.3, p. 113–126, 2002.

ASLAM, M.; KALYAR, M. A.; RAZA, Z. A. Polyvinyl alcohol: A review of research status and use of polyvinyl alcohol based nanocomposites. Polymer Engineering & Science, v. 58, n. 12, p. 2119-2132, 2018.

ASTM. **D882-12: Standard test method for tensile properties of thin plastic sheeting**, 2012.

ASTM. **E96/E96M-13: Standard test methods for water vapor transmission of materiais**, 2013.

ATARÉS, L.; CHIRALT, A. Essential oils as additives in biodegradable films and coatings for active food packaging. **Trends in Food Science & Technology**, v. 48, p. 51-62, 2016. Disponível em: https://doi.org/10.1016/j.tifs.2015.12.001.

BARBALATA-MÂNDRU, M. *et al*. Poly(vinyl alcohol)/Plant Extracts Films: Preparation, Surface Characterization and Antibacterial Studies against Gram Positive and Gram Negative Bacteria. **Materials**, v. 15, p. 2493, 2022. Disponível em: https://doi.org/10.3390/ma15072493.

BOF, M. J. *et al.* Bio-packaging material impact on blueberries quality attributes under transport and marketing conditions. **Polymers**, v. 13, n. 4, p. 481, 2021. Disponível em: https://doi.org/10.3390/polym13040481.

CARVALHO, F. A. *et al.* Polyvinyl alcohol films with different degrees of hydrolysis and polymerization. **Semina: Ciências Exatas e Tecnológicas**, Londrina, v. 40, n. 2, p. 169-178, 2019.

DAS, S. *et al*. The antibacterial and aroma finishing of cotton fabrics by Menthe pipertia extract. **Journal of Textile Institute**, v. 112, p. 1180-1190, 2021.

DE AZEREDO, H.M.C. Nanocomposites for food packaging applications. **Food Res**. v. 42, p. 1240–1253, 2009.

DE MELO, R.H.C.; CONCI, A., Succolarity: defining a method to calculate this fractal measure. *In*: **15th International Conference on Systems, Signals and Image Processing**, Bratislava, Slovakia, 22 August 2008.

ECHEVERRÍA, J.; ALBUQUERQUE, R.D.D.G. Nanoemulsions of essential oils: new tool for control of vector-borne diseases and in vitro effects on some parasitic agents. **Medicines**, v. 6, p. 42–53, 2019.

FERREIRA, I.M. *et al*. Ethylic Biodiesel Production Using Lipase Immobilized in Silk Fibroin-Alginate Spheres by Encapsulation. **Catal Letters**, v. 147, p. 269–280, 2017. Disponível em: https://doi.org/10.1007/s10562-016-1917-0

FIROUZ, M. S.; MOHI-ALDEN, K.; OMID, M. A critical review on intelligent and active packaging in the food industry: Research and development. **Food Research International**, v. 141, p. 110113, 2021.

GALDEANO, M. C.; WILHELM, A. E.; MALI, S.; GROSSMANN, M. V. E. Influence of thickness on properties of plasticized oat starch films. **Braz. Arch. Biol. Technol**., v. 56, p. 637-644, 2013.

GHANI, S. *et al*. The preparation, characterization and in vitro application evaluation of soluble soybean polysaccharide films incorporated with cinnamon essential oil nanoemulsions. **International Journal of Biological Macromolecules**, v. 112, p. 197–202, 2018.

GODOVSKY, D.Y. Device Applications of PolymerNanocomposites. *In*: **Biopolymers PVA Hydrogels, Anionic Polymerisation Nanocomposites**, Springer, Berlin, v. 163, 2000.

GUIMARÃES JUNIOR, M.; TEIXEIRA, F. G.; TONOLI, G. H. D. Effect of the nano-fibrillation of bamboo pulp on the thermal, structural, mechanical and

physical properties of nanocomposites based on starch/poly (vinyl alcohol) blend. **Cellulose**, v. 25, p. 823-1849, 2018.

HALIMA, N. B. Poly (vinyl alcohol): review of its promising applications and insights into biodegradation. **RSC advances**, v. 6, n. 46, p. 39823-39832, 2016.

JAMOVI PROJECT. **Jamovi. Versão 1.8**. Software de computador, 2021. Disponível em: https://www.jamovi.org.

JU, J. *et al.* Application of essential oil as a sustained release preparation in food packaging. **Trends Food Sci. Technol.**, v. 92, p. 22–32, 2019.

KANATT, S. R. *et al*. Active chitosan–polyvinyl alcohol films with natural extracts. **Food hydrocolloids**, v. 29, n. 2, p. 290-297, 2012.

KUCHAIYAPHUM, P. *et al.* Hydrophobicity enhancement of the polyvinyl alcohol/rice starch/silk fibroin films by glycerol. **Applied Mechanics and Materials**, v. 446, p. 360-365, 2014.

LI, Z. *et al*. Preparation, characterization and anti-aflatoxigenic activity of chitosan packaging films incorporated with turmeric essential oil. **International journal of biological macromolecules**, v. 131, p. 420-434, 2019.

LIMA, G. G. *et al*. Extraction method plays critical role in antibacterial activity of propolis-loaded hydrogels. **J. Pharm. Sci.**, v. 105, p. 1248–1257, 2016.

MANDELBROT, B. **The fractal geometry of nature**. New York: W. H. Freeman and company, 1983.

MANE, K. A. A Review on Active Packaging: An Innovation in Food Packaging. **International Journal of Environment, Agriculture and Biotechnology**. v. 1, n. 3, p. 544 - 549, 2016.

MASŁOWSKI, M. *et al.* Potential Application of Peppermint (Mentha piperita L.), German Chamomile (Matricaria chamomilla L.) and Yarrow (Achillea millefolium L.) as Active Fillers in Natural Rubber Biocomposites. **Int. J.Mol. Sci**. v.22, p. 7530, 2021.

MASSON, D. S. **Atividades cicatrizante e antimicrobiana do óleo-resina de copaíba (Copaifera langsdorffii) em úlceras cutâneas**. 2011. 215 p. Tese (Doutorado em Ciências Médicas) – Faculdade de

Medicina de Ribeirão Preto, Universidade de São Paulo, Ribeirão Preto, 2011.

MATOS, R.S. *et al.* 3D micromorphology evaluation of kefir microbial films loaded with extract of amazon rainforest fruit cupuacu, **Micron**, v. 142, p. 102996, 2021. https://doi.org/10.1016/j.micron.2020.102996

MATOS, R.S. *et al*. Advanced micromorphology study of microbial films grown on Kefir loaded with Açaí extract. **Micron**, v. 137, p. 102912, 2020. https://doi.org/10.1016/j.micron.2020.102912.

MUSTAFA, P. *et al*. Improving functional properties of PVA/starch-based films as active and intelligent food packaging by incorporating propolis and anthocyanin. **Polym. Polym. Compos**., v. 29, n. 9, p. 1472-1484, 2021.

OLEWNIK-KRUSZKOWSKA, E. *et al*. Antibacterial Films Based on PVA and PVA–Chitosan Modified with Poly(Hexamethylene Guanidine). **Polymers**, 11, 2093, 2019.

PARLINSKA-WOJTAN, M. *et al*. Green synthesis and antibacterial effects of aqueous colloidal solutions of silver nanoparticles using camomile terpenoids as a combined reducing and capping agent. **Bioprocess. Biosyst. Eng.**, v. 39, p. 1213-1223, 2016.

PAVIA, D. L. *et al*. **Introdução à Espectroscopia**. Tradução da 4ª ed. norte-americana. São Paulo: Cengage Learning, 2010.

PINHEIRO, J. G. O. *et al*. Inclusion Complexes of Copaiba (Copaifera multijuga Hayne) Oleoresin and Cyclodextrins: Physicochemical Characterization and Anti-Inflammatory Activity. **International Journal of Molecular Sciences**, v. 18, n. 11, p. 2388, 2017.

PINTO, E. P. *et al*. Comparing the nanoscale topography and interface properties of chitosan films containing free and nano-encapsulated copaiba essential oil: An atomic force microscopy (AFM) and Fractal Geometry study. **Materials Today Communications**, v. 35, p. 105765, 2023b.

PINTO, E. P. *et al*. Influence of low and high glycerol concentrations on wettability and flexibility of chitosan biofilms. **Química Nova**, São Paulo, v. 41, n. 10, p. 1109-1116, 2018.

PINTO, E. P. *et al*. Nanoscale 3D Spatial Analysis of Zirconia Disc Surfaces Subjected to Different Laser Treatments. **Fractal and Fractional**, v. 7, p. 160, 2023a. Disponível em: https://doi.org/10.3390/fractalfract702016.

PINTO, E. P.; *et al*. Lacunarity exponent and Moran index: a complementary methodology to analyze AFM images and its application to chitosan films. **Physica A: Statistical Mechanics and its Applications**, v. 581, p. 126192, 2021.

QUEMEL, G. K. C. *et al*. Propriedades medicinais do óleo da Copaifera Langsdorfii: uma revisão integrativa da literatura. **Brazilian Journal of Health Review**, v. 4, n. 3, p. 10490-10508, 2021.

REHMAN, A. *et al*. Development of active food packaging via incorporation of biopolymeric nanocarriers containing essential oils. **Trends in Food Science & Technology**, v. 101, p. 106-121, 2020.

SATHIDEVI, O. G. Structural properties and its significance of PVA. **International Journal of Scientific & Technology Research**, v. 9, n. 2, 2020.

SCATOLINO, M. V. *et a*l. Copaiba oil and vegetal tannin as functionalizing agents for açai nanofibril films: valorization of forest wastes from Amazonia. **Environmental Science and Pollution Research**, v. 29, n. 44, p. 66422-66437, 2022.

SUN, X. *et al*. Enhanced antimicrobial cellulose/chitosan/ZnO biodegradable composite membrane. **Membranes**, v. 12, n. 239, 2022.

TĂLU, S. *et al*. Advanced fractal analysis of nanoscale topography of Ag/DLC composite synthesized by RF-PECVD. Surface Engineering, v. 36, p. 713–719, 2020.

TANWAR, R. *et al*. Development and characterization of PVA-starch incorporated with coconut shell extract and sepiolite clay as an antioxidant film for active food packaging applications. **International Journal of Biological Macromolecules**, v. 185, p. 451-461, 31 ago. 2021. DOI: 10.1016/j.ijbiomac.2021.06.179.

TAO, G. *et al*. Biosynthesis and Characterization of AgNPs–Silk/PVA Film for Potential Packaging Application. **Materials**, v. 10, p. 667, 2017. Disponível em: https://doi.org/10.3390/ma10060667.

TAVARES-DIAS, M.; *et al*. In vitro anthelminthic activity of Lippia alba essential oil combined with silk fibroin against monogeneans of Colossoma macropomum (Serrasalmidae). **Aquaculture Research**, v. 52, n. 00, p. 1-6, 2021.

VAR, I.; UZUNLU, S. (Ed.). **Active antimicrobial food packaging**. BoD–Books on Demand, 2019.

VARGHESE, S. A. *et al*. Antimicrobial active packaging based on PVA/Starch films incorporating basil leaf extracts. **Materials Today: Proceedings**, v. 72, p. 3056-3062, 2023.

VEIGA JR., V. F.; PINTO, A. C.; O GÊNERO Copaifera L. **Química Nova**, v. 25, p. 273, 2002.

WYROSTEK, J. *et al*. Estimation of the Content of Selected Active Substances in Primary and Secondary Herbal Brews by UV-VIS and GC-MS Spectroscopic Analyses. **J. Anal. Methods Chem.**, v. 11, p. 8891855, 2020.

WYRWA, J; BARSKA, A. Packaging as a source of information about food products. **Procedia Engineering**, v. 182, p. 770-779, 2017.

YAMAGUCHI, M. H.; GARCIA, R. F. Óleo de copaíba e suas propriedades medicinais: revisão bibliográfica. **Revista Saúde e Pesquisa**, v. 5, n. 1, p. 137-146, 2012.

ZHEN, N. *et al*. Protein-based natural antibacterial materials and their applications in food preservation. **Microbial biotechnology**, v. 15, n. 5, p. 1324-1338, 2022.

ZHANG, Y.; SUNDARARAJAN, S. The effect of autocorrelation length on the real area of contact and friction behavior of rough surfaces. **Journal of applied physics**, v.97, p. 103526, 2005.